HOMOGENIZATION METHODOLOGY FOR THE LOW-ORDER EQUATIONS OF THE QUASIDIFFUSION METHOD

Dmitriy Y. Anistratov
Department of Nuclear Engineering
North Carolina State University
Raleigh, NC 27695-7909
anistratov@ncsu.edu

ABSTRACT

In this paper the development of spatial homogenization procedure is considered. Such procedure must preserve the averaged reaction rates, surface-averaged group currents, and eigenvalue. The coarse-mesh discretization of the low-order quasidiffusion equations that is consistent with a fine-mesh discretization is presented. The resulting scheme preserves also the first and second spatial Legendre moments of the fine-mesh transport solution. The definition of discontinuity factors is formulated. The theorem of consistency is proven. The numerical solution of the proposed method reproduces accurately the large-scale behavior of the transport solution within assembly. Numerical results that demonstrate efficiency of the proposed methodology are presented.

1. INTRODUCTION

The present generation of reactor analysis methodology uses the diffusion approximation in the full-core calculation; this can be significantly inaccurate at interfaces between different assemblies. In this paper we consider methodology based on the quasidiffusion equations, which can capture transport effects to an arbitrary degree of accuracy, and develop corresponding homogenization procedure for these equations.

The quasidiffusion (QD) method is an efficient method for solving particle transport problems [1, 2, 3, 4, 5]. The basic idea behind the QD method is to effectively reduce the dimensionality of the problem by averaging the transport equation over angular and energy variables, and closing equivalently the resulting system of equations by means of linear-fractional functionals. The resulting nonlinear problem of the QD method is equivalent to the original linear transport problem. The QD method is defined by a system of equations consisting of two parts: the transport (high-order) and moments (low-order) equations.

The homogenization fits naturally into the framework of the QD method, which is based on the idea of successively averaging the transport equation over angular and energy variables. Averaging over the spatial variable is the next logical step [3, 6]. The homogenization procedure must preserve the averaged reaction rates, surface-averaged group currents, and eigenvalue [7]. Here we present a coarse-mesh finite-element discretization of the QD low-order equations that is consistent with a fine-mesh discretization in such sense and is also able to preserve exactly two extra spatial moments of the fine-mesh transport solution over the coarse mesh (e.g., assembly or quarter assembly).

2. THE FEW-GROUP LOW-ORDER EQUATIONS OF THE QUASIDIFFUSION METHOD

To demonstrate the proposed homogenization approach, we consider a few-group k-eigenvalue transport problem for 1D slab geometry with vacuum boundary conditions. The low-order QD (LOQD) equations [3, 4] for the group scalar flux ϕ^g and current J^g are

$$\frac{d}{dx}J^g + \Sigma_t^g \phi^g = \sum_{p=1}^{M_g} \Sigma_{s,0}^{p\to g}\phi^p + \frac{1}{k_{eff}}\chi^g \sum_{p=1}^{M_g} \nu_f^p \Sigma_f^p \phi^p \,, \tag{1}$$

$$\frac{d}{dx}\left(E^g\phi^g\right) + \Sigma_t^g J^g = 0 \,, \tag{2}$$

$$J^g(0) = C_L^g \phi^g(0) \,, \quad J^g(X) = C_R^g \phi^g(X) \,, \tag{3}$$

$$0 \le x \le X \,, \quad g = 1, ..., M_g \,. \tag{4}$$

The functionals E^g, C_L^g and C_R^g are calculated by means of the few-group transport solution

$$E^g = \int_{-1}^{1}\mu^2\psi^g d\mu \Big/ \int_{-1}^{1}\psi^g d\mu \,,\; C_L^g = \int_{-1}^{0}\mu\psi^g d\mu \Big/ \int_{-1}^{0}\psi^g d\mu \Bigg|_{x=0} \,,\; C_R^g = \int_{0}^{1}\mu\psi^g d\mu \Big/ \int_{0}^{1}\psi^g d\mu \Bigg|_{x=X} \tag{5}$$

where ψ^g is the group angular flux. The LOQD problem (1)-(3) is equivalent to the original transport problem, and it exactly reproduces the transport solution.

3. FINE-MESH TRANSPORT SOLUTION AND ITS ASSEMBLY-LEVEL LARGE-SCALE BEHAVIOR

We discretize spatially the few-group low-order QD equations using a second-order finite-volume scheme [8]. A spatial fine mesh is defined by

$$\Omega^{fm} = \{x_{i-1/2}^{fm},\; i = 1, ..., N_x^{fm}+1,\; x_{1/2}^{fm} = 0,\; x_{N_x^{fm}+1/2}^{fm} = X\} \,, \tag{6}$$

and $h_i = x_{i+1/2}^{fm} - x_{i-1/2}^{fm}$ is the width of the ith cell. Integer $\pm\frac{1}{2}$ subscripts refer to cell-edge quantities, and integer subscripts refer to cell-average quantities. The difference scheme for the low-order equations of the QD method is defined by

$$J_{i+1/2}^{g,fm} - J_{i-1/2}^{g,fm} + \Sigma_{t,i}^g h_i \phi_i^{g,fm} = h_i \sum_{p=1}^{M_g} \Sigma_{s,0,i}^{p\to g}\phi_i^{p,fm} + h_i \frac{\chi_i^g}{k_{eff}^{fm}} \sum_{p=1}^{M_g} \nu_{f,i}^p \Sigma_{f,i}^p \phi_i^{p,fm} \,, \tag{7}$$

$$E_i^g \phi_i^{g,fm} - E_{i-1/2}^g \phi_{i-1/2}^{g,fm} + \frac{1}{2}\Sigma_{t,i}^g h_i J_{i-1/2}^{g,fm} = 0 \,, \tag{8}$$

$$E_{i+1/2}^g \phi_{i+1/2}^{g,fm} - E_i^g \phi_i^{g,fm} + \frac{1}{2}\Sigma_{t,i}^g h_i J_{i+1/2}^{g,fm} = 0 \,, \tag{9}$$

$$J_{1/2}^{g,fm} = C_L^g \phi_{1/2}^{g,fm} \,, \quad J_{N+1/2}^{g,fm} = C_R^g \phi_{N_x^{fm}+1/2}^{g,fm} \,, \tag{10}$$

$$i = 1, ..., N_x^{fm} \ .$$

As a result, we have the fine-mesh transport solution of the considered problem defined by fine-mesh eigenvalue k_{eff}^{fm}, grid functions of fine-mesh scalar flux $\phi_h^{g,fm}$, and current $J_h^{g,fm}$, which are defined as the following sets of numbers

$$J_h^{g,fm} = \{J_{i-1/2}^{g,fm}, i = 1, ..., N_x^{fm} + 1\} \ , \tag{11}$$

$$\phi_h^{g,fm} = \{\phi_i^{g,fm}, i = 1, ..., N_x^{fm};\ \phi_{j-1/2}^{g,fm}, i = 1, ..., N_x^{fm} + 1\} \ . \tag{12}$$

Note that the proposed methodology is applicable in general case when the fine-mesh transport solution is obtained by means of a transport differencing method that preserves particle balance in each cell, i.e. satisfies Eq. (7).

To demonstrate an example of the detailed structure of fine-mesh transport solution, we present the thermal scalar flux in a model MOX assembly next to uranium one. The considered assembly consists of 8 fuel pins separated by water. Figure 1 shows the fine-mesh scalar flux in the assembly, along with pin-cell average values of the scalar flux represented as a histogram plot. These results show that the large-scale behavior of the scalar flux within assemblies is characterized by a set of its pin-cell average values. The coarse-mesh solution should mimic this large-scale behavior in order to describe accurately the spatial shape of the scalar flux within assemblies. Figure 1 also shows the expansion of the solution in three Legendre polynomials (quadratic). Note that the few-term expansion captures efficiently the necessary large-scale features of the detailed assembly transport solution. We postulate that it is important for the coarse-mesh solution to preserve extra spatial moments of the fine-mesh solution in addition to zeroth moment; in this paper we define a coarse-mesh algorithm that produces such a "consistent" solution. It is conceivable that this consistency could actually degrade the accuracy of a coarse-mesh solution in some problems by causing it to over- or under-shoot at coarse-mesh surfaces. In this paper's fairly realistic test problems, the new consistent approach produces remarkable accuracy with no hint of over- or under-shoot. If difficulties arise in other problems, we believe that we can address them satisfactorily.

It is not necessary for a coarse-mesh solution to achieve precise pin powers on its own. Pin-power reconstruction uses the product of the coarse-mesh global solution and a "form function." This function is the pin-wise ratio of a single-assembly transport solution to a single-assembly coarse-mesh solution. If the single-assembly solution is perfect, then even a very crude coarse-mesh method will yield perfect reconstructed pin powers. The ultimate goal is for the reconstructed pin powers to be accurate even when the single-assembly problem is far from reality. The way to achieve that goal is to put more physics into the coarse-mesh solution and thus minimize the correction applied by the form function. The work presented here is intended to be a step toward that goal.

4. COARSE-MESH DISCRETIZATION: MAIN CONCEPTS

We define the following coarse mesh

$$\Omega^{cm} = \{x_{j-1/2},\ j = 1, ..., N_x^{cm} + 1,\ x_{1/2} = 0,\ x_{N_x^{cm}+1/2} = X\} \ , \tag{13}$$

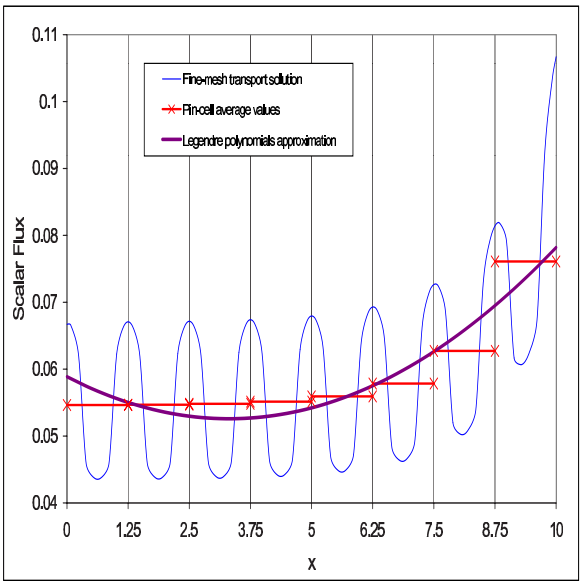

Figure 1: The structure of fine-mesh scalar flux in a model assembly.

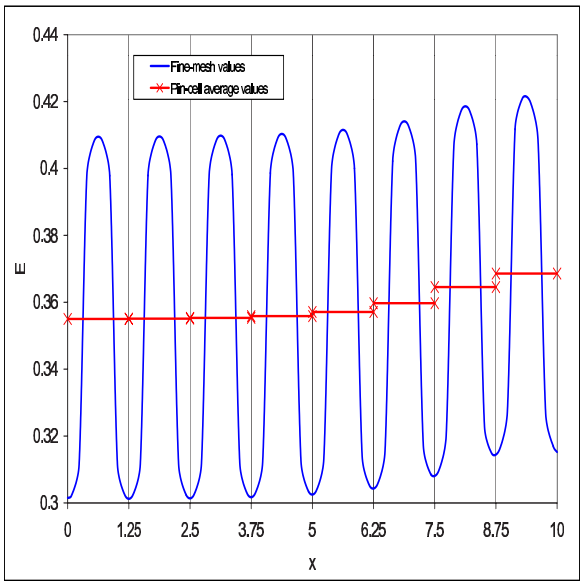

Figure 2: The structure of the fine-mesh QD functional E^g in a model assembly.

and a set of indices of fine cells that belong to the jth coarse-mesh interval $\omega_j = \{i : i_j^- \le i \le i_j^+\}$, where i_j^- and i_j^+ are the indices of the fine-mesh cells adjacent to the left and right boundary of the jth coarse interval, respectively, i.e. $x_{j-1/2} = x^{fm}_{i_j^- - 1/2}$. The width of the jth coarse-mesh interval is $H_j = x_{j+1/2} - x_{j-1/2}$.

To discretize the LOQD equations on a coarse mesh, we use a finite-element method based on the following expansion of the coarse-mesh scalar flux $\Phi_j(x)$ ($x_{j-1/2} \le x \le x_{j+1/2}$)

$$\Phi_j^g(x) = \sum_{l=0}^{2}(2l+1)\varphi_j^{(l),g} P_l(\zeta_j(x)) + \varphi_j^{(3),g}\sinh(\varkappa_j^g(x-x_j)) + \varphi_j^{(4),g}\cosh(\varkappa_j^g(x-x_j))\,, \quad (14)$$

where P_l are Legendre polynomials:

$$P_0(\zeta_j(x)) = 1, \quad P_1(\zeta_j(x)) = \zeta_j(x), \quad P_2(\zeta_j(x)) = \frac{1}{2}\left(3\zeta_j(x)^2 - 1\right), \quad (15)$$

$$\zeta_j(x) = \frac{2(x-x_j)}{H_j}, \quad x_j = 0.5(x_{j+1/2} + x_{j-1/2}), \quad 1 \le j \le N_x^{cm}\,, \quad (16)$$

and

$$\varkappa_j^g = \sqrt{\frac{(\langle\Sigma_t\rangle_j^g - \langle\Sigma_{s,0}\rangle_j^{g\to g})\langle\Sigma_t\rangle_j^g}{\langle E\rangle_j^g}}\,, \quad (17)$$

$$\langle\Sigma_t\rangle_j^g = \sum_{i\in\omega_j}\Sigma_{t,i}^g\phi_i^{g,fm}h_i \Big/ \sum_{i\in\omega_j}\phi_i^{g,fm}h_i\,, \quad (18)$$

$$\langle \Sigma_s \rangle_j^{p\to g} = \sum_{i\in\omega_j} \Sigma_{s,0,i}^{p\to g} \phi_i^{p,fm} h_i \Big/ \sum_{i\in\omega_j} \phi_i^{p,fm} h_i \,, \tag{19}$$

$$\langle E \rangle_j^{g} = \sum_{i\in\omega_j} E_i^{g} \phi_i^{g,fm} h_i \Big/ \sum_{i\in\omega_j} \phi_i^{g,fm} h_i \,. \tag{20}$$

The discretization scheme for the LOQD equations (1) and (2) can be formulated by means of a set of coarse-cell spatial moment equations of the balance equation (1), cell-edge approximation of the QD first-moment equation (2) and discontinuity conditions for the scalar flux. Let us first consider the case that the medium within each coarse-mesh interval is spatially uniform, and hence all cross sections are constant: $\Sigma_{\bullet,i}^{g} = \Sigma_{\bullet,j}^{g,*}$, $\nu_{f,i}^{g} = \nu_{f,j}^{g,*}$, $\chi_i^g = \chi_j^{g,*}$, and $\Sigma_{s,0,i}^{p\to g} = \Sigma_{s,0,j}^{p\to g,*}$ for $i \in \omega_j$. To derive a scheme for the LOQD equations (1) and (2) in this case, we integrate the balance equation (1) with weights $P_l(\zeta_j(x))$ $l = 0, 1, 2$ over coarse interval $x_{j-1/2} \le x \le x_{j+1/2}$

$$\int_{x_{j-1/2}}^{x_{j+1/2}} P_l(\zeta_j(x)) \left(\frac{d}{dx} J^g + \Sigma_t^g \phi^g - \sum_{p=1}^{M_g} \Sigma_{s,0}^{p\to g} \phi^p - \frac{1}{k_{eff}} \chi^g \sum_{p=1}^{M_g} \nu_f^p \Sigma_f^p \phi^p \right) dx = 0 \,, \tag{21}$$

to get the discretized equations for spatial moments of the coarse-mesh scalar flux

$$\Phi_j^{(l),g} = \frac{1}{H_j} \int_{x_{j-1/2}}^{x_{j+1/2}} P_l(\zeta_j(x)) \Phi_j^g(x) dx \,. \tag{22}$$

Taking into account Eq. (2), we get

$$J_{j+1/2}^g - J_{j-1/2}^g + \Sigma_{t,j}^{g,*} H_j \Phi_j^{(0),g} = H_j \sum_{p=1}^{M_g} \Sigma_{s,0,j}^{p\to g,*} \Phi_j^{(0),p} + H_j \frac{\chi_j^{g,*}}{k_{eff}} \sum_{p=1}^{M_g} \nu_{f,j}^{p,*} \Sigma_{f,j}^{p,*} \Phi_j^{(0),p} \,, \tag{23}$$

$$J_{j+1/2}^g + J_{j-1/2}^g + \frac{2}{\Sigma_{t,j}^{g,*} H_j} \Big(E^g(x_{j+1/2}) \Phi_j^g(x_{j+1/2}) - E^g(x_{j-1/2}) \Phi_j^g(x_{j-1/2}) \Big) +$$

$$\Sigma_{t,j}^{g,*} H_j \Phi_j^{(1),g} = H_j \sum_{p=1}^{M_g} \Sigma_{s,0,j}^{p\to g,*} \Phi_j^{(1),p} + H_j \frac{\chi_j^{g,*}}{k_{eff}} \sum_{p=1}^{M_g} \nu_{f,j}^{p,*} \Sigma_{f,j}^{p,*} \Phi_j^{(1),p} \,, \tag{24}$$

$$J_{j+1/2}^g - J_{j-1/2}^g + \frac{6}{\Sigma_{t,j}^{g,*} H_j} \Big(E^g(x_{j+1/2}) \Phi_j^g(x_{j+1/2}) + E^g(x_{j-1/2}) \Phi_j^g(x_{j-1/2}) - 2\langle E \rangle_j^g \Phi_j^{(0),g} \Big) +$$

$$\Sigma_{t,j}^{g,*} H_j \Phi_j^{(2),g} = H_j \sum_{p=1}^{M_g} \Sigma_{s,0,j}^{p\to g,*} \Phi_j^{(2),p} + H_j \frac{\chi_j^{g,*}}{k_{eff}} \sum_{p=1}^{M_g} \nu_{f,j}^{p,*} \Sigma_{f,j}^{p,*} \Phi_j^{(2),p} \,. \tag{25}$$

The approximation of the QD first moment equation (2) on the edges of the jth coarse cell have the form

$$E^g(x_{j-1/2}) \left. \frac{d\Phi_j^g}{dx} \right|_{x=x_{j-1/2}} + \Phi_j^g(x_{j-1/2}) \left. \frac{dE^g}{dx} \right|_{x=x_{j-1/2}} + \Sigma_{t,j}^{g,*} J_{j-1/2}^g = 0 \,, \tag{26}$$

$$E^g(x_{j+1/2})\left.\frac{d\Phi_j^g}{dx}\right|_{x=x_{j+1/2}} + \Phi_j^g(x_{j+1/2})\left.\frac{dE^g}{dx}\right|_{x=x_{j+1/2}} + \Sigma_{t,j}^{g,*} J_{j+1/2}^g = 0\,, \tag{27}$$

$$j = 1, ..., N_x^{cm}\,.$$

The discontinuity conditions for the scalar flux are

$$G_j^{g,+}\Phi_j^g(x_{j+1/2}) = G_{j+1}^{g,-}\Phi_{j+1}^g(x_{j+1/2})\,, \tag{28}$$

$$j = 1, ..., N_x^{cm} - 1\,,$$

where the discontinuity factors G will be defined later. The boundary conditions (3) result in the following equations:

$$J_{1/2}^g = C_L^g G_1^{g,-}\Phi_1^g(x_{1/2})\,, \quad J_{N_x^{cm}+1/2}^g = C_R^g G_{N_x^{cm}}^{g,+}\Phi_{N_x^{cm}}^g(x_{N_x^{cm}+1/2})\,. \tag{29}$$

In each cell the values of the functional $E^g(x_{j-1/2})$ and its derivative $\frac{dE^g}{dx}(x_{j-1/2})$ are defined by the fine-mesh solution. Provided that the discontinuity factors $G_j^{g,\pm}$ are specified, there are enough equations to determine uniquely coefficients of expansion $\varphi_j^{(l),g}$ and the currents $J_{j-1/2}^g$.

The presented scheme is able to preserve the values of fine-mesh currents and average values of the fine-mesh scalar flux over coarse-mesh intervals, i.e.

$$J_{j-1/2}^g = J_h^{g,fm}(x_{j-1/2})\,, \tag{30}$$

$$\Phi_j^{(0),g} = \frac{1}{H_j}\sum_{i\in\omega_j}\phi_i^{g,fm}h_i\,. \tag{31}$$

However, it does not preserve the first and second spatial moments of the fine-mesh scalar flux. A method that reproduces these extra moments can generate more accurate shape of the solution $\Phi_j^g(x)$ in realistic cases of heterogeneous media within areas covered by coarse intervals.

The goal of this paper is to derive a coarse-mesh discretization method for the LOQD equations that will generate a numerical solution that reproduces accurately the large-scale behavior of the transport solution within an assembly. To achieve this, one needs to obtain the discrete equations that will generate a coarse-mesh scalar flux solution whose first several spatial moments match exactly the corresponding moments of the fine-mesh scalar flux. This can be done by means of an algebraically consistent discretization.

Another issue is related to the way the coefficients of Eqs. (26) and (27) are defined in each assembly (coarse cell), to enable the coarse-mesh method to mimic the large-scale behavior of the transport solution characterized by pin-cell average values in an assembly. Figure 2 demonstrates the fine-mesh structure of the QD functional E^g in thermal group for the model assembly the solution of which was presented above in Fig. 1. From this figure we notice that if one uses the derivative of the QD functional E^g at the boundary calculated directly by means of small-scale solution, then the resulting values will not correspond to the large-scale behavior of the solution at all. Previous homogenization algorithms, including those by Smith [9], have used group data that is averaged over boundary pin cells. We will use similar approach for definition of some functionals necessary for coarse-mesh discretization of the LOQD equations.

5. CONSISTENT COARSE-MESH DICRETIZATION OF THE LOQD EQUATIONS

We consider the coarse-mesh discretization of the LOQD equations that is based on the expansion (14) of the scalar flux $\Phi_j^g(x)$ in each coarse interval $x_{j-1/2} \le x \le x_{j+1/2}$. The resulting scheme must preserve:

1. fine-mesh values of the currents at edges of coarse cells, i.e. $J^g_{j-1/2} = J_h^{g,fm}(x_{j-1/2})$, $j = 1, ..., N_x^{cm} + 1$,

2. zeroth, first and second spatial Legendre moments of the fine-mesh scalar flux over each coarse cell, i.e.
$$\Phi_j^{(l),g} = \phi_j^{(l),g,fm}\,, \quad l = 0, 1, 2\,, \tag{32}$$
where
$$\phi_j^{(l),g,fm} = \frac{1}{H_j} \sum_{i\in\omega_j} \bar{\mathcal{P}}_i^{l,j} \phi_i^{g,fm} h_i \tag{33}$$
is the discrete form of spatial Legendre moments of the fine-mesh scalar flux over $x_{j-1/2} \le x \le x_{j+1/2}$, $\phi_i^{g,fm}$ is the fine-mesh cell-average value of the scalar flux (Eq. (12)), and
$$\bar{\mathcal{P}}_i^{l,j} = \frac{1}{h_i} \int\limits_{x_{i-1/2}^{fm}}^{x_{i+1/2}^{fm}} P_l(\zeta_j(x))dx\,. \tag{34}$$

To derive spatial moments equations similar to Eq. (23)-(25) consistent with the fine-mesh discretization scheme (7)-(9), we perform the operation (21) of taking spatial moments of the balance equation (1) in discrete form by multiplying the fine-mesh discretized balance equation (7) by $\bar{\mathcal{P}}_i^{l,j}$ (l=0,1,2) and summing it over all fine-mesh cells that belong to the jth coarse interval
$$\sum_{i\in\omega_j} \bar{\mathcal{P}}_i^{l,j} \left(J_{i+1/2}^{g,fm} - J_{i-1/2}^{g,fm} \right) + \sum_{i\in\omega_j} \bar{\mathcal{P}}_i^{l,j} \Sigma_{t,i}^g \phi_i^{g,fm} h_i =$$
$$\sum_{p=1}^{M_g} \sum_{i\in\omega_j} \bar{\mathcal{P}}_i^{l,j} \Sigma_{s,0,i}^{p\to g} \phi_i^{p,fm} h_i + \frac{1}{k_{eff}} \sum_{p=1}^{M_g} \sum_{i\in\omega_j} \bar{\mathcal{P}}_i^{l,j} \chi_i^g \nu_{f,i}^p \Sigma_{f,i}^p \phi_i^{p,fm} h_i\,. \tag{35}$$

For l=0 Eq. (35) results in the coarse-mesh balance equation
$$J^g_{j+1/2} - J^g_{j-1/2} + \langle \Sigma_t \rangle_j^g H_j \Phi_j^{(0),g} = H_j \sum_{p=1}^{M_g} \langle \Sigma_{s,0} \rangle_j^{p\to g} \Phi_j^{(0),p} + \frac{H_j}{k_{eff}} \sum_{p=1}^{M_g} \langle \chi \nu_f \Sigma_f \rangle_j^{p,g} \Phi_j^{(0),p}\,, \tag{36}$$
$$j = 1, ..., N_x^{cm}\,,$$
where the spatially averaged cross sections are defined by (18), (19), and
$$\langle \chi \nu_f \Sigma_f \rangle_j^{p,g} = \sum_{i\in\omega_j} \chi_i^g \nu_{f,i}^p \Sigma_{f,i}^p \phi_i^{p,fm} h_i \Big/ \sum_{i\in\omega_j} \phi_i^{p,fm} h_i\,. \tag{37}$$

Let us assume now that the discontinuity factors $G_j^{g,\pm}$ are known. Equation (35) for l=1 is transformed equivalently to the following form:

$$J_{j+1/2}^g + J_{j-1/2}^g + \frac{2}{\langle\Sigma_t\rangle_j^g H_j}\left(E_j^{g,+}\Phi_j^g(x_{j+1/2}) - E_j^{g,-}\Phi_j^g(x_{j-1/2})\right) +$$

$$\left[\sum_{i\in\omega_j}\bar{\mathcal{P}}_i^{1,j}\left(J_{i+1/2}^{g,fm} - J_{i-1/2}^{g,fm}\right) - J_h^{g,fm}(x_{j+1/2}) - J_h^{g,fm}(x_{j-1/2}) -\right.$$

$$\left.\frac{2}{\langle\Sigma_t\rangle_j^g H_j}\left(E_j^{g,+}\frac{\phi_h^{g,fm}(x_{j+1/2})}{G_j^{g,+}} - E_j^{g,-}\frac{\phi_h^{g,fm}(x_{j-1/2})}{G_j^{g,-}}\right)\right] + \tag{38}$$

$$\langle\Sigma_t\rangle_j^g H_j\Phi_j^{(1),g} + \sum_{i\in\omega_j}\left[\Sigma_{t,i}^g - \langle\Sigma_t\rangle_j^g\right]\bar{\mathcal{P}}_i^{1,j}\phi_i^{g,fm}h_i =$$

$$H_j\sum_{p=1}^{M_g}\langle\Sigma_{s,0}\rangle_j^{p\to g}\Phi_j^{(1),p} + \sum_{p=1}^{M_g}\sum_{i\in\omega_j}\left[\Sigma_{s,0,i}^{p\to g} - \langle\Sigma_{s,0}\rangle_j^{p\to g}\right]\bar{\mathcal{P}}_i^{1,j}\phi_i^{p,fm}h_i +$$

$$\frac{H_j}{k_{eff}}\sum_{p=1}^{M_g}\langle\chi\nu_f\Sigma_f\rangle_j^{p,g}\Phi_j^{(1),p} + \frac{1}{k_{eff}}\sum_{p=1}^{M_g}\sum_{i\in\omega_j}\left[\chi_i^g\nu_{f,i}^p\Sigma_{f,i}^p - \langle\chi\nu_f\Sigma_f\rangle_j^{p,g}\right]\bar{\mathcal{P}}_i^{1,j}\phi_i^{p,fm}h_i\,,$$

where

$$E_j^{g,-} = E^g(x_{j-1/2})\,,\quad E_j^{g,+} = E^g(x_{j+1/2})\,. \tag{39}$$

Note that the term in large square brackets is zero if $J_{j-1/2}^g = J_h^{g,fm}(x_{j-1/2})$, $\Phi_j^{(1),g} = \phi_j^{(1),g,fm}$, and $G_j^{g,\pm} = \phi_h^{g,fm}(x_{j\pm1/2})/\Phi_j^g(x_{j\pm1/2})$. To formulate the final form of the discrete first moment equation in terms of spatial moments of the coarse-mesh scalar flux, we define the following functionals

$$\alpha_j^{(1),g} = \left[\sum_{i\in\omega_j}\bar{\mathcal{P}}_i^{1,j}\left(J_{i+1/2}^{g,fm} - J_{i-1/2}^{g,fm}\right) - J_h^{g,fm}(x_{j+1/2}) - J_h^{g,fm}(x_{j-1/2}) -\right.$$

$$\left.\frac{2}{\langle\Sigma_t\rangle_j^g H_j}\left(E_j^{g,+}\frac{\phi_h^{g,fm}(x_{j+1/2})}{G_j^{g,+}} - E_j^{g,-}\frac{\phi_h^{g,fm}(x_{j-1/2})}{G_j^{g,-}}\right)\right] \Bigg/ \sum_{i\in\omega_j}\phi_i^{g,fm}h_i\,, \tag{40}$$

$$\beta_{t,j}^{(1),g} = \sum_{i\in\omega_j}\left[\Sigma_{t,i}^g - \langle\Sigma_t\rangle_j^g\right]\bar{\mathcal{P}}_i^{1,j}\phi_i^{g,fm}h_i \Bigg/ \sum_{i\in\omega_j}\phi_i^{g,fm}h_i\,, \tag{41}$$

$$\beta_{s,j}^{(1),p\to g} = \sum_{i\in\omega_j}\left[\Sigma_{s,0,i}^{p\to g} - \langle\Sigma_{s,0}\rangle_j^{p\to g}\right]\bar{\mathcal{P}}_i^{1,j}\phi_i^{p,fm}h_i \Bigg/ \sum_{i\in\omega_j}\phi_i^{p,fm}h_i\,, \tag{42}$$

$$\beta_{f,j}^{(1),p,g} = \sum_{i\in\omega_j}\left[\chi_i^g\nu_{f,i}^p\Sigma_{f,i}^p - \langle\chi\nu_f\Sigma_f\rangle_j^{p,g}\right]\bar{\mathcal{P}}_i^{1,j}\phi_i^{p,fm}h_i \Bigg/ \sum_{i\in\omega_j}\phi_i^{p,fm}h_i\,. \tag{43}$$

Using Eqs. (40)-(43), the equation (38) is reduced to

$$J^g_{j+1/2} + J^g_{j-1/2} + \frac{2}{\langle\Sigma_t\rangle^g_j H_j}\left(E^{g,+}_j\Phi^g_j(x_{j+1/2}) - E^{g,-}_j\Phi^g_j(x_{j-1/2})\right) +$$

$$\langle\Sigma_t\rangle^g_j H_j\Phi^{(1),g}_j + \left(\alpha^{(1),g}_j + \beta^{(1),g}_{t,j}\right)H_j\Phi^{(0),g}_j = \tag{44}$$

$$H_j\sum_{p=1}^{M_g}\langle\Sigma_{s,0}\rangle^{p\to g}_j\Phi^{(1),p}_j + \frac{H_j}{k_{eff}}\sum_{p=1}^{M_g}\langle\chi\nu_f\Sigma_f\rangle^{p,g}_j\Phi^{(1),p}_j + H_j\sum_{p=1}^{M_g}\left(\beta^{(1),p\to g}_{s,j} + \frac{1}{k_{eff}}\beta^{(1),p,g}_{f,j}\right)\Phi^{(0),p}_j\,,$$

$$j = 1, ..., N^{cm}_x\,.$$

Similarly, to transform the equation (35) for l=2, we define the functionals

$$\alpha^{(2),g}_j = \left[\sum_{i\in\omega_j}\bar{\mathcal{P}}^{2,j}_i\left(J^{g,fm}_{i+1/2} - J^{g,fm}_{i-1/2}\right) - J^{g,fm}_h(x_{j+1/2}) + J^{g,fm}_h(x_{j-1/2}) -\right.$$

$$\left.\frac{6}{\langle\Sigma_t\rangle^g_j H_j}\left(E^{g,+}_j\frac{\phi^{g,fm}_h(x_{j+1/2})}{G^{g,+}_j} + E^{g,-}_j\frac{\phi^{g,fm}_h(x_{j-1/2})}{G^{g,-}_j} - 2\langle E\rangle^g_j\phi^{(0),g,fm}_j\right)\right]\Bigg/\sum_{i\in\omega_j}\phi^{g,fm}_i h_i\,, \tag{45}$$

$$\beta^{(2),g}_{t,j} = \sum_{i\in\omega_j}\left[\Sigma^g_{t,i} - \langle\Sigma_t\rangle^g_j\right]\bar{\mathcal{P}}^{2,j}_i\phi^{g,fm}_i h_i\Bigg/\sum_{i\in\omega_j}\phi^{g,fm}_i h_i\,, \tag{46}$$

$$\beta^{(2),p\to g}_{s,j} = \sum_{i\in\omega_j}\left[\Sigma^{p\to g}_{s,0,i} - \langle\Sigma_{s,0}\rangle^{p\to g}_j\right]\bar{\mathcal{P}}^{2,j}_i\phi^{p,fm}_i h_i\Bigg/\sum_{i\in\omega_j}\phi^{p,fm}_i h_i\,, \tag{47}$$

$$\beta^{(2),p,g}_{f,j} = \sum_{i\in\omega_j}\left[\chi^g_i\nu^p_{f,i}\Sigma^p_{f,i} - \langle\chi\nu_f\Sigma_f\rangle^{p,g}_j\right]\bar{\mathcal{P}}^{2,j}_i\phi^{p,fm}_i h_i\Bigg/\sum_{i\in\omega_j}\phi^{p,fm}_i h_i\,. \tag{48}$$

As a result, we get the discretized second spatial moment equation of the form

$$J^g_{j+1/2} - J^g_{j-1/2} + \frac{6}{\langle\Sigma_t\rangle^g_j H_j}\left(E^{g,+}_j\Phi^g_j(x_{j+1/2}) + E^{g,-}_j\Phi^g_j(x_{j-1/2}) - 2\langle E\rangle^g_j\Phi^{(0),g}_j\right) +$$

$$\langle\Sigma_t\rangle^g_j H_j\Phi^{(2),g}_j + \left(\alpha^{(2),g}_j + \beta^{(2),g}_{t,j}\right)H_j\Phi^{(0),g}_j = \tag{49}$$

$$H_j\sum_{p=1}^{M_g}\langle\Sigma_{s,0}\rangle^{p\to g}_j\Phi^{(2),p}_j + \frac{H_j}{k_{eff}}\sum_{p=1}^{M_g}\langle\chi\nu_f\Sigma_f\rangle^{p,g}_j\Phi^{(2),p}_j + H_j\sum_{p=1}^{M_g}\left(\beta^{(2),p\to g}_{s,j} + \frac{1}{k_{eff}}\beta^{(2),p,g}_{f,j}\right)\Phi^{(0),p}_j\,,$$

$$j = 1, ..., N^{cm}_x\,.$$

Next we formulate the relationship between the current, the scalar flux and its derivative at the coarse-cell edges that is based on Eq. (2)

$$\langle E\rangle^{g,L}_j\left.\frac{d\Phi^g_j}{dx}\right|_{x=x_{j-1/2}} + \left\langle\frac{dE}{dx}\right\rangle^{g,L}_j\Phi^g_j(x_{j-1/2}) + \langle\Sigma_t\rangle^{g,L}_j J^g_{j-1/2} = 0\,, \tag{50}$$

$$\langle E\rangle_j^{g,R}\left.\frac{d\Phi_j^g}{dx}\right|_{x=x_{j+1/2}} + \left\langle\frac{dE}{dx}\right\rangle_j^{g,R}\Phi_j^g(x_{j+1/2}) + \langle\Sigma_t\rangle_j^{g,R}J_{j+1/2}^g = 0\,, \tag{51}$$

$$j = 1, ..., N_x^{cm}\,.$$

where to define the coefficients of these equations, we use pin-cell average data. Consider that there are Z_j pin cells in the jth coarse interval and

$$\langle\Sigma_t\rangle_j^{g,pin\#m} = \sum_{i\in\omega_j^{pin\#m}}\Sigma_{t,i}^g\phi_i^{g,fm}h_i \Big/ \sum_{i\in\omega_j^{pin\#m}}\phi_i^{g,fm}h_i\,, \tag{52}$$

$$\langle E\rangle_j^{g,pin\#m} = \sum_{i\in\omega_j^{pin\#m}}E_i^g\phi_i^{g,fm}h_i \Big/ \sum_{i\in\omega_j^{pin\#m}}\phi_i^{g,fm}h_i \tag{53}$$

are the total cross section and QD functional E^g averaged over the mth pin cell of the jth coarse interval, where $\omega_j^{pin\#m}$ is a set of indices of fine-mesh intervals that belong to the mth pin cell.

$$H_j^{pin\#m} = \sum_{i\in\omega_j^{pin\#m}}h_i \tag{54}$$

is the width of the mth pin cell. In Eqs. (50) and (51) the functional E^g and total cross section are averaged over boundary pin cells

$$\langle E\rangle_j^{g,L} = \langle E\rangle_j^{g,pin\#1}\,, \quad \langle E\rangle_j^{g,R} = \langle E\rangle_j^{g,pin\#Z_j}\,, \tag{55}$$

$$\langle\Sigma_t\rangle_j^{g,L} = \langle\Sigma_t\rangle_j^{g,pin\#1}\,, \quad \langle\Sigma_t\rangle_j^{g,R} = \langle\Sigma_t\rangle_j^{g,pin\#Z_j}\,, \tag{56}$$

and

$$\left\langle\frac{dE}{dx}\right\rangle_j^{g,L} = 2\left(\langle E\rangle_j^{g,pin\#2} - \langle E\rangle_j^{g,pin\#1}\right)\Big/\left(H_j^{pin\#2} + H_j^{pin\#1}\right)\,, \tag{57}$$

$$\left\langle\frac{dE}{dx}\right\rangle_j^{g,R} = 2\left(\langle E\rangle_j^{g,pin\#Z_j} - \langle E\rangle_j^{g,pin\#Z_j-1}\right)\Big/\left(H_j^{pin\#Z_j} + H_j^{pin\#Z_j-1}\right)\,. \tag{58}$$

The equations (50) and (51) with group data defined by (55)-(58) enable us to approximate the large-scale behavior of the transport solution next to the boundaries of coarse intervals. To complete the system of discretized equations of the proposed method, we define the discontinuity conditions for the scalar flux

$$G_j^{g,+}\Phi_j^g(x_{j+1/2}) = G_{j+1}^{g,-}\Phi_{j+1}^g(x_{j+1/2})\,, \quad j = 1, ..., N_x^{cm} - 1\,, \tag{59}$$

and boundary conditions (3)

$$J_{1/2}^g = C_L^g G_1^{g,-}\Phi_1^g(x_{1/2})\,, \quad J_{N_x^{cm}+1/2}^g = C_R^g G_{N_x^{cm}}^{g,+}\Phi_{N_x^{cm}}^g(x_{N_x^{cm}+1/2})\,. \tag{60}$$

As a result, the system of the coarse-mesh discretized LOQD equations consists of

1. the balance equation (36),

2. the first spatial moment equation (44),
3. the second spatial moment equation (49),
4. two interface equations (50) and (51),
5. the discontinuity conditions (59),
6. the QD boundary conditions (60).

Substituting the expansion (14) into these equations, one obtains the final set of algebraic equations for $\varphi_j^{(l),g}$, $l = 0, ..., 4$, $j = 1, ..., N_x^{cm}$ and $J_{j-1/2}^g$, $j = 1, ..., N_x^{cm} + 1$, $(g = 1, ..., M_g)$.

6. DEFINITION OF DISCONTINUITY FACTORS AND THEOREM OF CONSISTENCY

To define the discontinuity factors $G_j^{g,\pm}$ for the proposed discretization method, we introduce an auxiliary function

$$\widehat{\Phi}_j^g(x) = \sum_{l=0}^{2}(2l+1)\widehat{\varphi}_j^{(l),g}P_l(\zeta_j(x)) + \widehat{\varphi}_j^{(3),g}\sinh(\varkappa_j^g(x-x_j)) + \widehat{\varphi}_j^{(4),g}\cosh(\varkappa_j^g(x-x_j)) \qquad (61)$$

which is the solution of Eqs. (36), (44), (49)-(51) for the jth coarse cell such that it reproduces the average value of the fine-mesh scalar flux, the first and second spatial Legendre moments of the fine-mesh scalar flux, and currents on edges of this coarse cell. To calculate the coefficients of expansion of $\widehat{\Phi}_j^g(x)$, we need to solve the following set of equations in terms of $\varphi_j^{(l),g}$, $l = 0, ..., 4$ in the jth cell:

$$\langle E\rangle_j^{g,L}\left.\frac{d\widehat{\Phi}_j^g}{dx}\right|_{x=x_{j-1/2}} + \left\langle\frac{dE}{dx}\right\rangle_j^{g,L}\widehat{\Phi}_j^g(x_{j-1/2}) = -\langle\Sigma_t\rangle_j^{g,L}J_h^{g,fm}(x_{j-1/2})\,, \qquad (62)$$

$$\langle E\rangle_j^{g,R}\left.\frac{d\widehat{\Phi}_j^g}{dx}\right|_{x=x_{j+1/2}} + \left\langle\frac{dE}{dx}\right\rangle_j^{g,R}\widehat{\Phi}_j^g(x_{j+1/2}) = -\langle\Sigma_t\rangle_j^{g,R}J_h^{g,fm}(x_{j+1/2})\,, \qquad (63)$$

$$\widehat{\Phi}_j^{(l),g} = \phi_j^{(l),g,fm}\,, \quad l = 0, 1, 2\,. \qquad (64)$$

The discontinuity factors are defined as the ratio

$$G_j^{g,\pm} = \phi_h^{g,fm}(x_{j\pm1/2})\Big/\widehat{\Phi}_j^g(x_{j\pm1/2})\,. \qquad (65)$$

Thus, to calculate the discontinuity factors, we solve a set of auxiliary discrete equations (62)-(64) using the known fine-mesh solution obtained from assembly-level calculations, and hence we do not need to solve a complete transport problem in homogenized zones (assemblies).

Theorem

The coarse-mesh discrete low-order QD equations (36), (44), (49)-(51), (59), and (60), with discontinuity factors (65), cross sections and functionals defined by (18)-(20), (37), (39)-(43),(45)-(48), (55)-(58) are consistent with the given transport differencing method that generates the reference fine-mesh transport solution $\phi_h^{g,fm}$ and $J_h^{g,fm}$ in the sense that the coarse-mesh

solution $\Phi_j^g(x)$ preserves the average value of the fine-mesh scalar flux and reaction rates over each coarse-mesh cell, the first and second spatial Legendre moments of the fine-mesh scalar flux over coarse intervals, fine-mesh currents at edges of coarse cells, and fine-mesh k-eigenvalue, i.e.

$$\Phi_j^{(l),g} = \phi_j^{(l),g,fm}\,, \quad l = 0,1,2\,. \quad J_{j-1/2}^g = J_h^{g,fm}(x_{j-1/2})\,, \quad k_{eff} = k_{eff}^{fm}\,, \tag{66}$$

$$\langle \Sigma_t \rangle_j^g H_j \Phi_j^{(0),g} = \sum_{i\in\omega_j} \Sigma_{t,i}^g \phi_i^{g,fm} h_i\,, \quad \langle \Sigma_{s,0} \rangle_j^{p\to g} H_j \Phi_j^{(0),p} = \sum_{i\in\omega_j} \Sigma_{s,0,i}^{p\to g} \phi_i^{p,fm} h_i\,, \tag{67}$$

$$\langle \chi\nu_f\Sigma_f \rangle_j^{p,g} H_j \Phi_j^{(0),p} = \sum_{i\in\omega_j} \chi_i^g \nu_{f,i}^p \Sigma_{f,i}^p \phi_i^{p,fm} h_i\,. \tag{68}$$

Proof

We constructed the auxiliary function $\widehat{\Phi}_j^g(x)$ in a such way that it preserves the zeroth, first and second spatial Legendre moments of the fine-mesh scalar flux over coarse intervals as well as the fine-mesh currents on edges of coarse cells. If one calculates $\alpha_j^{(l),g}$, $l = 1,2$ (Eqs.(40) and (45)) using $G_j^{g,\pm}$ defined by (65) , and substitutes $\widehat{\Phi}_j^g(x)$ into Eqs. (36), (44), (49)-(51), (59), and (60), then it is easy to see that it satisfies these coarse-mesh discretized equations. Thus, $\Phi_j^g(x) = \widehat{\Phi}_j^g(x)$ and $\Phi_j^g(x)$ meets the conditions (66). Then, the definition of spatially averaged cross sections (Eqs. (18), (19) and (37)) leads to (67) and (68). ■

7. ASSEMBLY-LEVEL TRANSPORT CALCULATIONS

The proposed method can be used in combination with assembly-level transport calculations that utilize albedo boundary conditions, without making color-set calculations, to simulate interaction with adjacent assembly in a reactor core [10]. Note that most reactor analysis is presently based on transport calculations of assembly with reflective boundary conditions. Note further that if the albedo boundary conditions accurately represent the presence of a different neighboring assembly, then the single-assembly transport calculation accurately reproduces the correct fine-mesh solution, and all functionals calculated from single-assembly solution will be accurate.

Let us consider that each coarse-mesh cell represents a whole assembly. To generate fine-mesh transport solution for a given assembly (coarse cell) and calculate the averaged cross sections and functionals for the few-group coarse-mesh discretized LOQD equations, we perform a set of single-assembly transport calculations on fine spatial mesh with albedo boundary conditions ($0 \le x \le X$)

$$\psi^g(0,\mu) = \gamma_L^g(\mu)\psi^g(0,-\mu)\,, \text{ for } \mu > 0\,, \quad \psi^g(X,\mu) = \gamma_R^g(\mu)\psi^g(X,-\mu)\,, \text{ for } \mu < 0 \tag{69}$$

where γ_L^g, γ_R^g are albedos. The resulting boundary conditions for the few-group LOQD equations have the following form [6]:

$$J^g(0) = \frac{1-\lambda_{L,1}^g}{1+\lambda_{L,0}^g} C_L^g \phi^g(0)\,, \quad \lambda_{L,n}^g = \int_{-1}^0 \mu^n \gamma_L^g(-\mu)\psi^g(0,\mu)d\mu \Big/ \int_{-1}^0 \mu^n \psi^g(0,\mu)d\mu\,, \tag{70}$$

$$J^g(X) = \frac{1-\lambda^g_{R,1}}{1+\lambda^g_{R,0}} C^g_R \phi^g(X) \ , \quad \lambda^g_{R,n} = \int_0^1 \mu^n \gamma^g_R(-\mu)\psi^g(X,\mu)d\mu \Big/ \int_0^1 \mu^n \psi^g(X,\mu)d\mu \ , \qquad (71)$$

where $n = 0, 1$. In this methodology various albedos are used to simulate interface phenomena between different assemblies.

8. NUMERICAL RESULTS

To demonstrate the efficiency of the developed methodology, we present numerical results from two test problems that simulate interaction of uranium and MOX fuel assemblies in 1D slab geometry with two energy groups. In these test problems we use model uranium and MOX assemblies [9]. There are two half-assemblies next to each other with reflective boundary conditions on the outside. A MOX half-assembly is on the left and a uranium half-assembly is on the right. Each assembly contains only one kind of fuel pin cells, with 8 pin cells per assembly. The half-assembly width is 10 cm. The design of a fuel pin is shown on Figure 3. Two tests differ only in their fuel cross sections, which are listed in Table 1 and 2. The fine mesh solutions were calculated by the QD method using the second order finite-volume scheme for the LOQD equations described above (Eqs.(7)-(10)) and step characteristic method for the transport equation to calculate the QD functionals [8]. The fine mesh consists of 128 equal cells ($N_x^{fm} = 128$), and hence 8 cells per pin cell. The angular mesh has 10 intervals. The multiplication factors in tests A and B equal 1.5. The coarse mesh consists of one cell per half-assembly; thus, $N_x^{cm} = 2$.

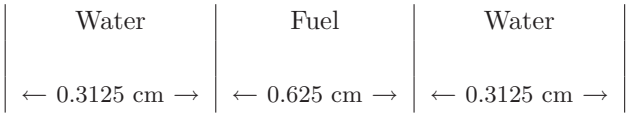

Figure 3: Pin cell design.

Figures 4-11 display numerical results of Tests A and B. The fine-mesh scalar fluxes, their pin-cell average values, and coarse-mesh solutions obtained by means of the proposed method are shown in Figures 4, 5, 8, and 9. The spatial distribution of the fine-mesh QD functionals and their pin-cell average values are presented in Figures 6, 7, 10, and 11. The graphs demonstrate that the resulting coarse-mesh scalar flux approximates accurately the large-scale behavior of the transport solution within assemblies characterized by the pin-cell average values. Tables 3 and 4 present the relative difference in pin-cell average values of the fine-mesh transport solution and coarse-mesh LOQD solution. In Test A, the largest relative differences in the fast group for the MOX and uranium assemblies are $-7{\cdot}10^{-4}$ and $5{\cdot}10^{-4}$, respectively. In the thermal group, the largest relative differences are $-4{\cdot}10^{-3}$ and $-2{\cdot}10^{-2}$ for MOX and uranium assemblies, correspondingly. The maximum relative difference is in the thermal scalar flux of the uranium assembly at the interface. In Test B, the maximum relative difference between two solutions is smaller. The relative differences of the solutions at assemblies interface in thermal group are $-3{\cdot}10^{-3}$ and $-1{\cdot}10^{-3}$, for MOX and uranium assemblies, correspondingly. These numerical results show that the relative difference in pin-cell average values of the fine-mesh transport and

coarse-mesh LOQD solutions is small, and, thus, the proposed method generates an accurate coarse-mesh solution. This means that the coarse-mesh solution needs very little correction from the form function in order to produce very accurate pin powers.

Table 1: Test A. Cross Sections Data.

Cross Sections	Σ_t^1	$\Sigma_{s,0}^{1\to1}$	$\Sigma_{s,0}^{1\to2}$	Σ_f^1	ν_f^1	Σ_t^2	$\Sigma_{s,0}^{2\to2}$	$\Sigma_{s,0}^{2\to1}$	Σ_f^2	ν_f^2
MOX fuel	0.2	0.2	0	0	0	0.6	0	0	0.6	1.5
Uranium fuel	0.2	0.2	0	0	0	0.2	0	0	0.2	1.5
Water	0.2	0.17	0.03	0	0	1.1	1.1	0	0	0

Table 2: Test B. Cross Sections Data.

Cross Sections	Σ_t^1	$\Sigma_{s,0}^{1\to1}$	$\Sigma_{s,0}^{1\to2}$	Σ_f^1	ν_f^1	Σ_t^2	$\Sigma_{s,0}^{2\to2}$	$\Sigma_{s,0}^{2\to1}$	Σ_f^2	ν_f^2
MOX fuel	0.2	0.185	0.015	0	0	1.2	0.9	0	0.3	1.5
Uranium fuel	0.2	0.185	0.015	0	0	1.0	0.9	0	0.1	1.5
Water	0.2	0.17	0.03	0	0	1.1	1.1	0	0	0

Table 3: Test A. Relative Difference in Pin-Cell Average Values.

g	Assembly	Pin # 1	Pin # 2	Pin # 3	Pin # 4	Pin # 5	Pin # 6	Pin # 7	Pin # 8
1	MOX	$-7\cdot10^{-4}$	$3\cdot10^{-5}$	$6\cdot10^{-4}$	$6\cdot10^{-4}$	$4\cdot10^{-5}$	$-5\cdot10^{-4}$	$-4\cdot10^{-4}$	$3\cdot10^{-4}$
1	U	$-3\cdot10^{-4}$	$-4\cdot10^{-4}$	$2\cdot10^{-4}$	$5\cdot10^{-4}$	$5\cdot10^{-4}$	$2\cdot10^{-4}$	$-2\cdot10^{-4}$	$-4\cdot10^{-4}$
2	MOX	$-4\cdot10^{-3}$	$-2\cdot10^{-3}$	$7\cdot10^{-4}$	$3\cdot10^{-3}$	$4\cdot10^{-3}$	$4\cdot10^{-3}$	$-3\cdot10^{-4}$	$-5\cdot10^{-3}$
2	U	$-2\cdot10^{-2}$	$1\cdot10^{-2}$	$1\cdot10^{-2}$	$2\cdot10^{-3}$	$-6\cdot10^{-3}$	$-7\cdot10^{-3}$	$-2\cdot10^{-3}$	$4\cdot10^{-3}$

Table 4: Test B. Relative Difference in Pin-Cell Average Values.

g	Assembly	Pin # 1	Pin # 2	Pin # 3	Pin # 4	Pin # 5	Pin # 6	Pin # 7	Pin # 8
1	MOX	$-7\cdot10^{-4}$	$1\cdot10^{-4}$	$8\cdot10^{-4}$	$6\cdot10^{-4}$	$-1\cdot10^{-4}$	$-7\cdot10^{-4}$	$-3\cdot10^{-4}$	$4\cdot10^{-4}$
1	U	$-2\cdot10^{-4}$	$-7\cdot10^{-4}$	$1\cdot10^{-4}$	$6\cdot10^{-4}$	$6\cdot10^{-4}$	$2\cdot10^{-4}$	$-2\cdot10^{-4}$	$-5\cdot10^{-4}$
2	MOX	$-3\cdot10^{-3}$	$-6\cdot10^{-4}$	$2\cdot10^{-3}$	$3\cdot10^{-3}$	$3\cdot10^{-3}$	$9\cdot10^{-4}$	$-2\cdot10^{-3}$	$-2\cdot10^{-3}$
2	U	$-1\cdot10^{-3}$	$-2\cdot10^{-4}$	$4\cdot10^{-5}$	$8\cdot10^{-4}$	$1\cdot10^{-3}$	$8\cdot10^{-4}$	$-2\cdot10^{-4}$	$1\cdot10^{-3}$

8. CONCLUSIONS

We have developed a coarse-mesh discretization of the low-order QD equations that is consistent with the given fine-mesh differencing method for the LOQD equations in the sense that it preserves average values of the fine-mesh scalar flux over the given coarse cells as well as reaction rates, the first and second spatial Legendre moments of the fine-mesh scalar flux over coarse intervals, currents at edges of coarse cells, and the fine-mesh multiplication factor. All these facts are rigorous mathematical results. The definition of discontinuity factors has been derived. The

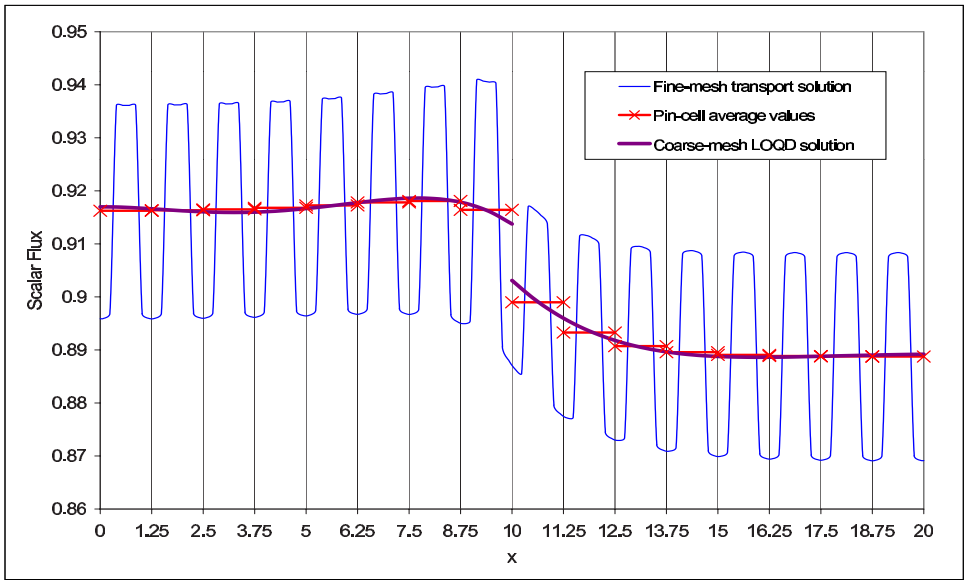

Figure 4: Test A. The fast scalar flux versus position.

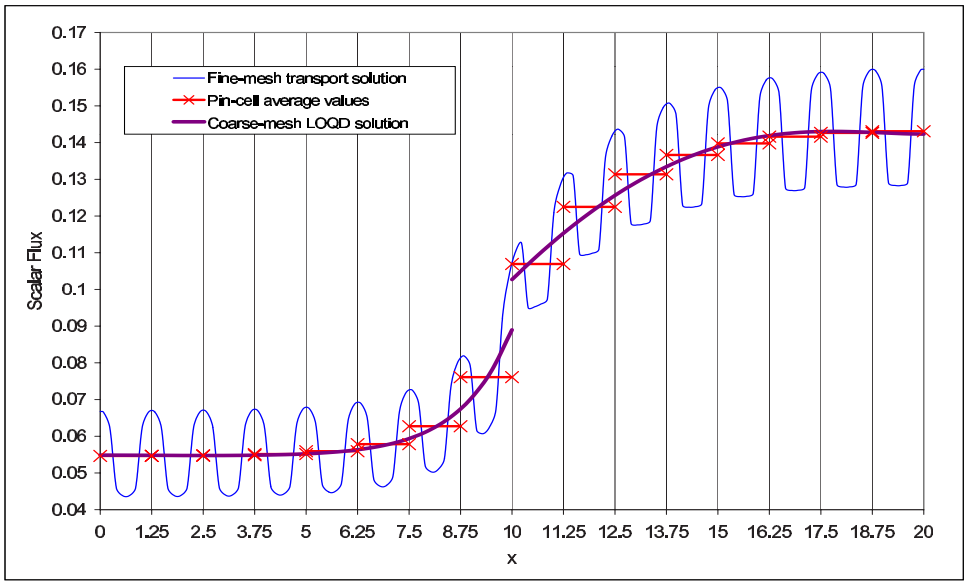

Figure 5: Test A. The thermal scalar flux versus position.

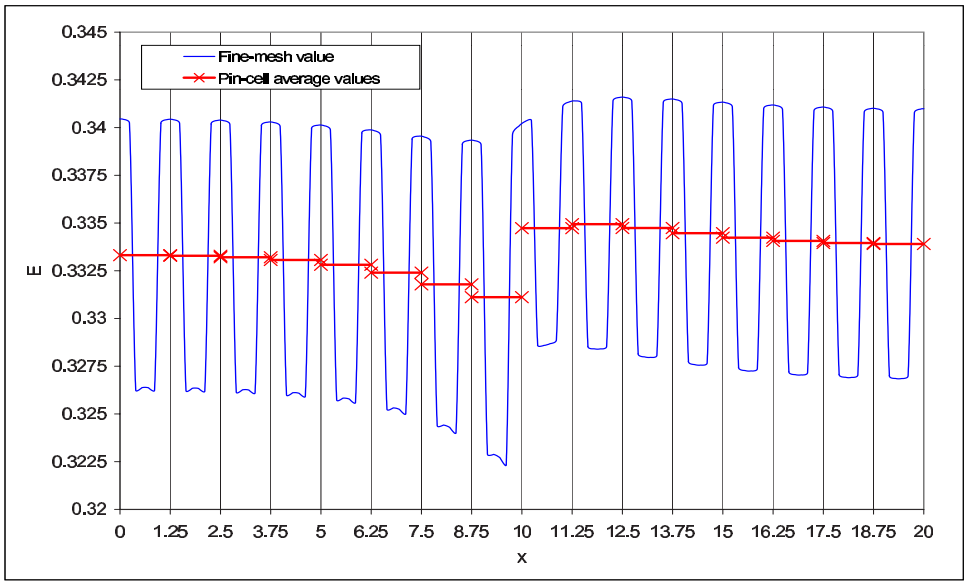

Figure 6: Test A. The fast group QD functional (E^1) versus position.

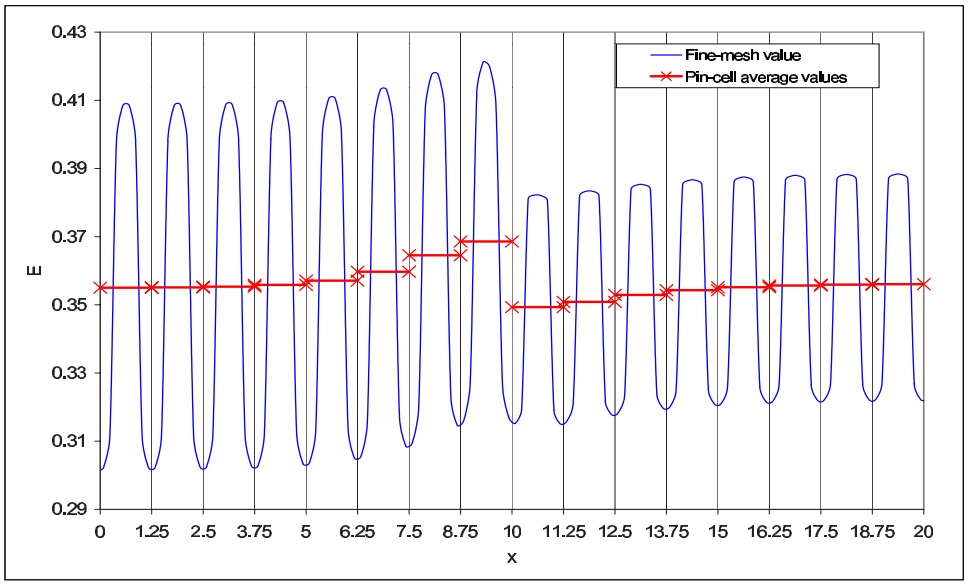

Figure 7: Test A. The thermal group QD functional (E^2) versus position.

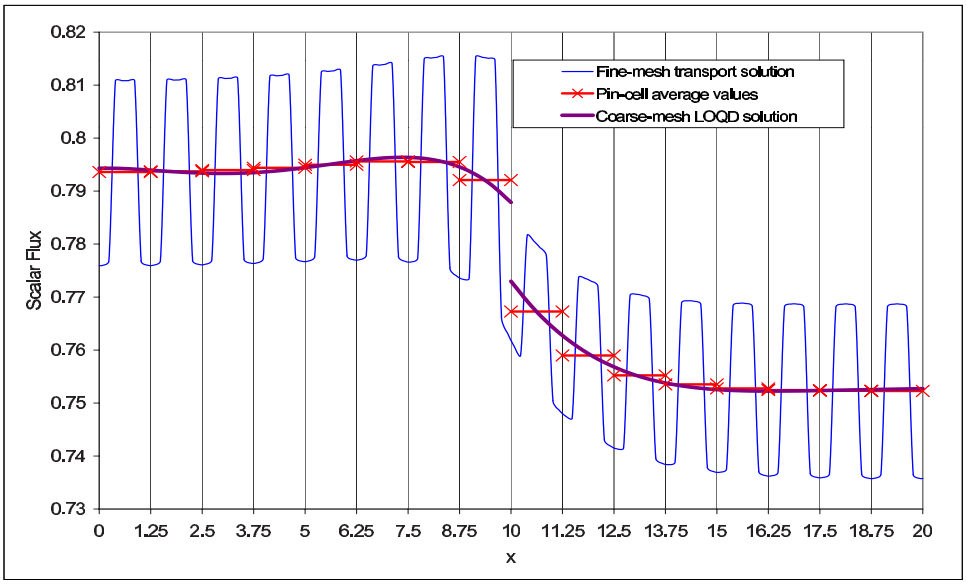

Figure 8: Test B. The fast scalar flux versus position.

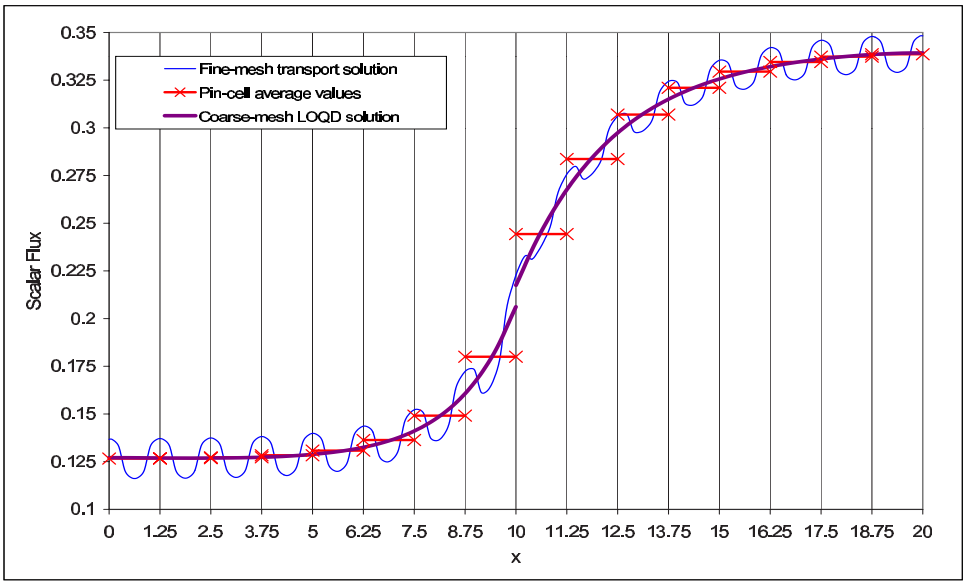

Figure 9: Test B. The thermal scalar flux versus position.

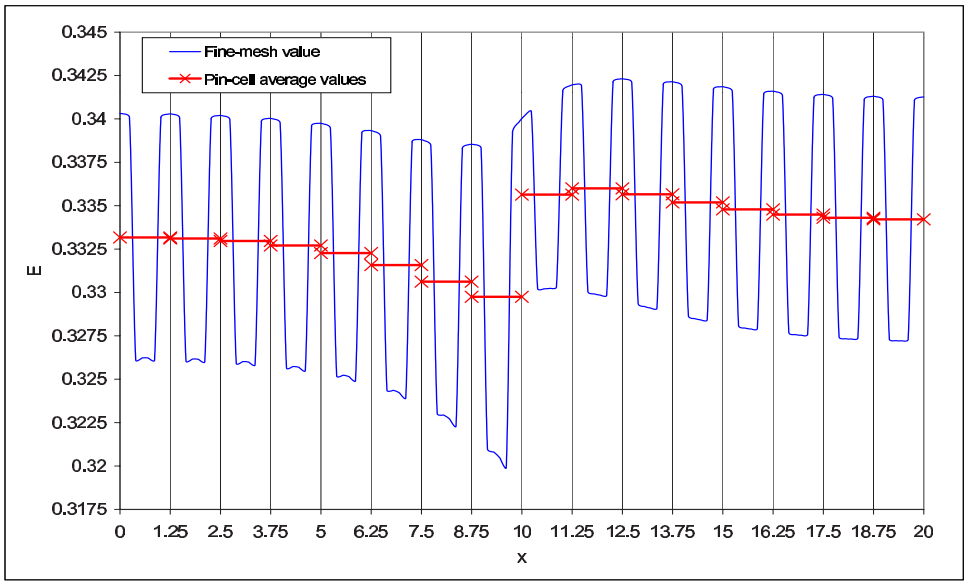

Figure 10: Test B. The fast group QD functional (E^1) versus position.

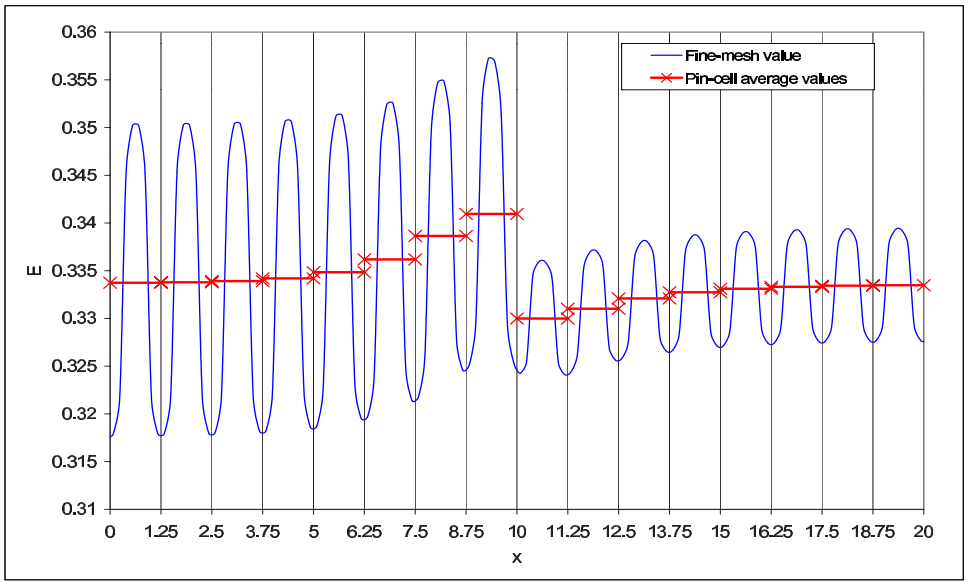

Figure 11: Test B. The thermal group QD functional (E^2) versus position.

resulting discretization scheme enables one to approximate accurately the large-scale behavior of the transport solution within assemblies.

The developed method can be applied to a general transport method as well, if this method preserves the particle balance. If a fine-mesh solution is obtained directly from a transport differencing method, and it is used to calculate spatially averaged cross sections and functionals defined in this paper, then the resulting coarse-mesh solution of the LOQD equations will be consistent with the given transport method. The reason is that the coarse-mesh scheme was derived by algebraically consistent discretization based on the discrete particle balance equation (7), and thus this scheme works also for any transport method whose solution satisfies the discrete balance equation (7).

The results from our test problems are extremely encouraging: the coarse-mesh scalar fluxes almost perfectly match every fine-mesh pin-cell average flux, in both the fast and thermal groups. However, we recognize that the test problems presented here are limited, especially in that each assembly has uniform pin cells. Enrichment variations, burnable absorbers, water holes, etc. could introduce within-assembly flux variations that could conceivably cause our moment-matching solution to lose accuracy. We will explore this question in the near future and modify our method if necessary, attempting to retain the strengths that it so obviously displays.

In closing, we note that the proposed methodology can be extended to multidimensional geometries and finite-element methods based on higher-order expansions of the coarse-mesh scalar flux. We are working now on such extensions. We also note that the proposed coarse-mesh algorithm must be coupled with other parts of a complete reactor-analysis methodolgy (generation of tables of constants, interpolation using tables, pin-power reconstruction). The full new methodology must then be compared against the existing state of the art. We are currently working on this implementation and testing.

ACKNOWLEDGEMENTS

The author thanks Marvin Adams, Kord Simth and Todd Palmer for helpful discussions. This work was supported by Nuclear Energy Research Initiative (NERI) Program of the US Department of Energy under grant No. DE-FG03-99SF21922.

References

[1] V.Ya. Gol'din, "A Quasidiffusion Method for Solving the Kinetic Equation," *USSR Comp. Math. and Math. Phys.* **4**, 136-149 (1964).

[2] N. N. Aksenov and V. Ya. Gol'din, "Computation of the Two-Dimensional Stationary Equation of Neutron Transfer by the Quasi-Diffusion Method," *USSR Comp. Math. and Math. Phys.*, **19**, No. 5, 263-266 (1979).

[3] V. Ya. Gol'din, "On Mathematical Modeling of Problems of Non-Equilibrium Transfer in Physical Systems," in *Modern Problems of Mathematical Physics and Computational Mathematics*, Nauka, Moscow, 113-127 (1982) (in Russian).

[4] D. Y. Anistratov and V. Ya. Gol'din, "Solving the Multigroup Transport Equation by the Quasidiffusion Method," *Preprint of the Keldysh Institute for Applied Mathematics*, the USSR Academy of Sciences, No. 128 (1986) (in Russian).

[5] E.N.Aristova, V.Ya. Gol'din, and A.V.Kolpakov, "Multidimensional Calculations of Radiation Transport by Nonlinear Quasi-Diffusion Method," *Proceeding of ANS International Conference on Mathematics and Computation, Reactor Physics and Environmental Analysis in Nuclear Applications*, Sept. 27-30, 1999, Madrid, Spain, 667-676 (1999).

[6] D.Y. Anistratov and M.L. Adams, "Consistent Coarse-Mesh Discretization of the Low-Order Equations of the Quasidiffusion Method," *Trans. Am. Nucl. Soc.,* **83**, 250-251 (2000).

[7] K. S. Smith, "Assembly Homogenization Techniques for Light Water Reactor Analysis," *Progress in Nuclear Energy*, **17**, 303-335 (1986).

[8] D.Y. Anistratov and V.Ya. Gol'din, "Nonlinear Methods for Solving Particle Transport Problems," *Transport Theory Statist. Phys.* **22** 42–77 (1993).

[9] K. S. Smith, *private communication.*

[10] K.T. Clarno and M.L. Adams, "Improved Boundary Conditions for Assembly-Level Transport Calculations," this proceedings (2002).